Dynamic nuclear polarization in NMR

N. Chandrakumar

Abstract | Dynamic nuclear polarization was first predicted — and, shortly thereafter, established experimentally — in 1953, the first demonstration being on Lithium metal. The basic approach involves the saturation of the ESR of a paramagnetic species in the system, while the NMR is observed. Initial applications of DNP involved low and moderate field studies that focused especially on investigations of molecular hydrodynamics. Applications to MRI provided a subsequent fillip to the technique. In the meanwhile, the closely related nuclear Overhauser effect (NOE) — which involves saturation, as well as observation of different NMR signals — had become an essential technique for the structure elucidation of both small molecules, as well as biomolecules. Most recently, DNP is witnessing rejuvenation, with high field applications to sensitivity enhancement in NMR.

We present in the following an overview of Dynamic nuclear polarization (DNP). The elementary general theory of the phenomenon is discussed. Four different DNP mechanisms that are currently recognized are briefly introduced and different modes of the experiment — involving either cw ESR irradiation, or pulsed ESR excitation — are pointed out. A brief run down of various possible implementations is presented, including our own early work at moderate fields in cw mode, as well as hardware configurations and requirements for high field DNP. Different current implementations of DNP experiments are summarized, including solid state, as well as in situ and ex situ dissolution DNP variants. Typical results of DNP enhanced high resolution NMR are then briefly discussed, including the results of our own early work on differential ^{19}F enhancements at moderate fields. Design of free radicals that satisfy the requirements to establish an efficient cross effect DNP is discussed. Recent experiments that have succeeded in detecting an intermediate in the photocycle of bacteriorhodopsin are alluded to. Finally, the implementation of ultrafast multi-dimensional NMR techniques under DNP conditions is briefly discussed, as an approach to further exploitation of the prospects that are on offer.

1. Introduction

The sensitivity of NMR has always been a constraint, while the resolution associated with the technique, even in solid state, has been its forte. There has therefore been considerable motivation all along to improve the sensitivity of NMR without losing resolution significantly. Clearly, improved sensitivity would offer scope to investigate phenomena that would be otherwise inaccessible by NMR.

Among important methods for sensitivity enhancement, one may count the use of:

(i) ever higher magnetic field intensities B_0, which lead in principle to improvement of the

Department of Chemistry, Indian Institute of Technology, Madras, Chennai 600036, Tamil Nadu, India
nckumar@iitm.ac.in

Figure 1: The energy level diagram of a two-spin-1/2 system, comprising an electron (negative γ) and a nucleus (with γ assumed to be positive). The spin states of both particles are shown by the side of each energy level, the first symbol representing the state of the electron; an ordinal number is associated with each level, increasing with energy. Excess (or relative) populations are shown below or above the energy levels, while the probability of relaxation transitions — shown by double headed arrows — that are operative in solution state are indicated with the symbols W_i.

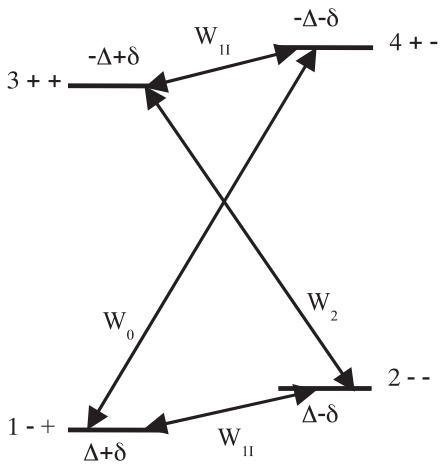

sensitivity (as defined by the signal-to-noise ratio) by the factor:

$$S/\mathcal{N} \sim N\gamma^{\frac{5}{2}} B_0^{\frac{3}{2}} \quad (1)$$

N being the number of spins per unit volume, of magnetogyric ratio γ;

(ii) cryoprobes[1,2] and cooled preamplifiers, which in principle reduce the thermal noise voltage in proportion to $T^{1/2}$, T being the temperature;

(iii) Polarization transfer from high γ, high abundance species in the spin system to improve the detection sensitivity of low γ low abundance species, in direct[3–8] as well as in indirect detection mode[9–16]; and

(iv) Dynamic nuclear polarization (DNP), by employing non-equilibrium populations created by microwave pumping of ESR in the system[17–19] or by chemical means, including CIDNP[20,21], parahydrogen induced polarization (PHIP)[22–26], or the use of other hyperpolarized gases, including ^{3}He or ^{129}Xe[27–29]. Optical enhancement strategies are also to be noted[30].

In this brief overview, we will discuss DNP generated by microwave pumping of ESR in the system, a strategy enabled for example by the addition of suitable paramagnetic species to the sample under investigation.

The sixties, seventies and eighties of the last century saw a good deal of activity in this area working at low and moderate fields, much emphasis being placed on the investigation of molecular dynamics by DNP measurements[31–34]. There was later a renaissance of very low field applications, for purposes of MRI[35]. In the last decade, however, DNP has been rejuvenated by high field applications[36–43]. In the following, we will briefly consider the basic principles both of low and moderate field DNP enhanced spectroscopy, as well as of high field DNP enhanced spectroscopy — and briefly summarize some of the applications and fascinating prospects.

Probably the only DNP work done in India thus far has been from the Indian Institute of Technology, Kanpur, in the Lab of Professor P.T. Narasimhan, during the mid-sixties to the mid-eighties[44–47]. As part of this effort, the present author designed and constructed during his years there a moderate resolution X-band DNP spectrometer[48] and investigated the DNP of ^{1}H and ^{19}F in diamagnetic solvents, interacting with a stable free radical solute such as tri-*t*-butyl phenoxyl (TTBP). The most interesting phenomenon uncovered was that of differential enhancements, at X-band, of different ^{19}F sites of the same molecule, owing to different scalar cross-relaxation rates; this was successfully modeled by the introduction of an sp_σ polarizability parameter[49,50]. In contrast, ^{1}H sites tended to exhibit DNP enhancements that were controlled by essentially non-selective dipolar cross relaxation. Some of the details of the spectrometer developed for this purpose, typical spectral output and differential enhancement results are briefly discussed later in this review.

2. Theory

Many of the basic features of DNP in solution state — and in solid state — may be understood by reference to the energy level diagram, shown in Fig. 1, of a pair of spins-1/2: an electron and a nuclear spin (with γ assumed positive for the nucleus in the following, without loss of generality).

Let us consider first the solution state situation when W_0 is the probability of the sole relaxation mechanism operating, equilibrating the relative populations of the levels numbered 1 and 4. Both the electron spin transitions are assumed to be saturated by irradiation, thus equalizing the populations within each of the pairs of levels 1–3 and 2–4; while, as mentioned earlier, W_0 maintains the thermal equilibrium population difference across the pair of levels 1–4. Let the equilibrium excess (or relative)

populations of the electron energy levels be $\pm\Delta$ and that of the nuclear spin energy levels be $\pm\delta$.

In calculating the redistributed populations under saturation, taking into account W_0 relaxation, the basic constraint to be satisfied is the conservation of the vanishing sum of the relative populations of the four energy levels:

$$N_1 + N_2 + N_3 + N_4 = 0 \quad (2)$$

The supplementary constraints that are to be satisfied by the redistributed populations under the conditions stipulated above are given by:

$$N_1 = N_3; \quad N_2 = N_4; \quad N_1 – N_4 = 2(\Delta + \delta) \quad (3)$$

This immediately results in:

$$N_4 = -(\Delta + \delta) = N_2, N_1 = (\Delta + \delta) = N_3 \quad (4)$$

As a consequence, the NMR transitions 1–2 and 3–4 now have the population difference $N_1 - N_2 = 2(\Delta + \delta) = N_3 - N_4$, in place of their equilibrium population differences which are both equal to 2δ. The relative enhancement of polarization η therefore amounts to:

$$\eta \equiv (\langle I_z \rangle - \langle I_0 \rangle)/\langle I_0 \rangle = (\Delta/\delta) \equiv -\gamma_e/\gamma_n \quad (5)$$

Note that this is in reality a positive enhancement: the observed spin I has been assumed to have the opposite sign of γ, relative to the saturated electron spin.

In exactly similar vein, one may readily infer that when the relaxation mechanism operative is the one that equilibrates the relative populations of the levels 2 and 3, W_2 being its probability, we have under conditions of ESR saturation:

$$N_1 = N_3; \quad N_2 = N_4; \quad N_2 - N_3 = 2(\Delta - \delta) \quad (6)$$

This results in the redistributed relative populations:

$$N_3 = -(\Delta - \delta) = N_1; \quad N_2 = (\Delta - \delta) = N_4 \quad (7)$$

Both the NMR transitions 1–2 and 3–4 now have the population difference $-2(\Delta - \delta)$, leading to a relative enhancement of polarization amounting to:

$$\eta = -(\Delta/\delta) \equiv \gamma_e/\gamma_n \quad (8)$$

It may be noted that the polarization is now opposite in sign to that achieved when W_0 is operative.

Finally, it is clear that when the relaxation mechanism operative is the one that equilibrates the relative populations of levels 1 and 2, as well as of levels 3 and 4, W_{1I} being its probability, the equilibrium polarizations are retained; this follows from its very definition.

The overall relative enhancement of polarization when both W_2 and W_0 are operative is therefore the probability weighted algebraic sum of the two individual relative enhancements, which is thus proportional to:

$$(W_2 - W_0)(\gamma_e/\gamma_n) \quad (9)$$

The actual relative enhancement is then clearly given by the ratio:

$$\eta = [(W_2 - W_0)/(W_0 + 2W_{1I} + W_2)](\gamma_e/\gamma_n) \quad (10)$$

In the solid state, the mechanism operative in dielectrics (as opposed to metallic conductors) to establish DNP is quite different and is termed the solid effect. This may however again be understood in terms of the basic two-spin-1/2 energy level diagram, this time invoking the saturation of either of the 'forbidden' transitions between levels 1 and 4 or between 2 and 3. Clearly, the extent to which such a forbidden transition may be excited depends on the mixing of states — and is therefore quite efficient at relatively low fields. Further, saturation of the 1–4 transition clearly leads to a negative enhancement, while saturation of the 2–3 transition leads to a positive enhancement.

Overhauser effect

At low and moderate fields, the DNP enhancement relates to the motional spectral density of the system, since the latter controls the relaxation transition rates. For efficient DNP, spectral density is required to occur at the electron Larmor frequency – or, more accurately, at its sum and difference with the nuclear Larmor frequency. The relative enhancement factor, as deduced above, is given by:

$$\eta \equiv \frac{\langle I_z \rangle - \langle I_0 \rangle}{\langle I_0 \rangle} = \left(\frac{W_2 - W_0}{W_0 + 2W_{1I} + W_2 + W^o} \right) \frac{\gamma_e}{\gamma_n} \quad (11)$$

Here, W's indicate the probability of the double, zero and single quantum relaxation processes as indicated by the subscript(s), I being the nuclear spin being observed (species n), while e is the electron spin being saturated. W^o is the probability of other relaxation processes that the nucleus may be subject to, not involving its scalar or dipolar interaction with the unpaired electron.

While this general formula is valid for any mixture of scalar and dipolar cross relaxation, it may be noted that for scalar cross relaxation alone, only W_0 is relevant. The enhancement factor under

these conditions amounts to $-(\gamma_e/\gamma_n)$, if W^o may be neglected.

In the case of dipolar cross relaxation under extreme narrowing conditions, on the other hand, one finds $W_0{:}2W_{1I}{:}W_2{::}1{:}3{:}6$, resulting in a relative enhancement of $(1/2)(\gamma_e/\gamma_n)$ when W^o is negligible.

The field dependence of DNP may be visualized readily, employing standard Lorentzian spectral density functions for the respective relaxation transition probabilities:

$$W_i \sim \frac{\tau_c}{1+\omega_i^2\tau_c^2} \tag{12}$$

Here, ω_i equals $\omega_e \pm \omega_n$, or $\omega_n$respectively for the zero, double and nuclear single quantum relaxation transitions, while τ_c is the motional correlation time. Clearly, given the high Larmor frequency of the electron, the enhancement drops dramatically at higher fields of operation, and vanishes when only W_{1I} is operative.

It has been recognized that scalar cross relaxation can however contribute to DNP enhancements at rather higher fields than can dipolar cross-relaxation[37,51]. Scalar cross relaxation may in turn be of two kinds, involving either the modulation of the hyperfine coupling between electron and nucleus (scalar relaxation of the first kind), or the rapid change of electron spin state (scalar relaxation of the second kind). However, the extent of the scalar contribution to DNP is once again reduced by a 'leakage factor' which corresponds to the relative weightage of other nuclear relaxation mechanisms, that are independent of the electron spin.

Fig. 2 depicts the dependence of the relative DNP enhancement η on the parameter $(\omega\tau_c)$, ω being the electron Larmor frequency, for the case of dipolar cross relaxation, as also for five different scalar cross relaxation scenarios in addition.

Solid effect

Not long after the prediction – and verification – of the Overhauser effect, an independent mechanism of DNP was observed in solids, and termed the solid effect[52–57]. The solid effect relies on the irradiation of a forbidden transition in an electron-nuclear coupled system as noted above, resulting in positive or negative enhancements of the nuclear spin transitions depending on which of the two forbidden transitions in the four level system is irradiated. If the two forbidden transitions overlap owing to a large inhomogeneous EPR linewidth, on the other hand, there could clearly be partial cancellation of the enhancement, a situation termed the differential solid effect. The solid effect also has an inverse field dependence, and requires that the inhomogeneous spread Δ, as well as homogenous linewidth δ of the electron spin resonance spectrum be smaller than the nuclear Larmor frequency: i.e., $\Delta, \delta < \omega_n$. The solid effect is characterized by the fact that the separation between the irradiation frequencies for maximum positive and negative enhancements is no less than twice the nuclear Larmor frequency. The integrated solid effect[58] avoids the cancellation of enhancements due to overlapping forbidden transitions, by recourse to electron spin inversion either by a π pulse, or preferably by adiabatic fast passage of the field.

Cross effect

Subsequently, DNP was observed in the solid state in systems where $\Delta > \omega_n > \delta$, the irradiation frequency separation between the maximum positive and negative enhancements now being less than $2\omega_n$; this phenomenon has been attributed to the cross effect[59–62], which involves two dipole coupled electron spins whose resonance frequencies differ by the nuclear Larmor frequency. Current efforts in high field DNP largely exploit the cross effect in solids, employing either a mixture of radicals, or a designer biradical suitably tethered to 'tune' the electron spin resonance frequencies to satisfy the required condition. The cross effect is at its most efficient at low temperatures. It may be visualized in terms of the energy level diagram of a three-spin-1/2 system comprising two electrons and a nuclear spin[42]. The theory and functional optimization of the cross effect is still a matter of further consolidation; recent efforts include the exploration of multi-photon strategies in this context[63].

Thermal mixing

Yet another regime in which DNP has been observed in the solid state is in systems where $\delta > \omega_n$, where the effect occurs by a thermal mixing mechanism[42,61,62]. This mechanism however appears not to be very promising for NMR applications because it requires a higher concentration of paramagnetic species, compromising as a result the NMR resolution.

Pulsed experiments

While most of the DNP experiments briefly introduced above may be performed in continuous wave (cw) ESR irradiation mode, saturating the electron spin resonance, it is also possible to invoke a generalized Hartmann-Hahn type transfer of polarization from electrons to nuclear spins in the time domain, e.g., by matching the electron nutation frequency under a microwave pulse (i.e., the Rabi

Figure 2: OE relative enhancement curves in units of $\gamma_{irr}/\gamma_{obs}$, as a function of $\omega\tau_c$ for dipolar and scalar cross relaxation, the latter with various values of the weightage factor k for 'other' nuclear relaxation mechanisms. ω is the electron Larmor frequency, while τ_c is the motional correlation time. Blue: dipolar cross relaxation; all other colors: scalar cross relaxation, for different values of k; green: $k=1$; red: $k=0.5$; cyan: $k=0.1$; purple: $k=0.01$; brown: $k=0.001$.

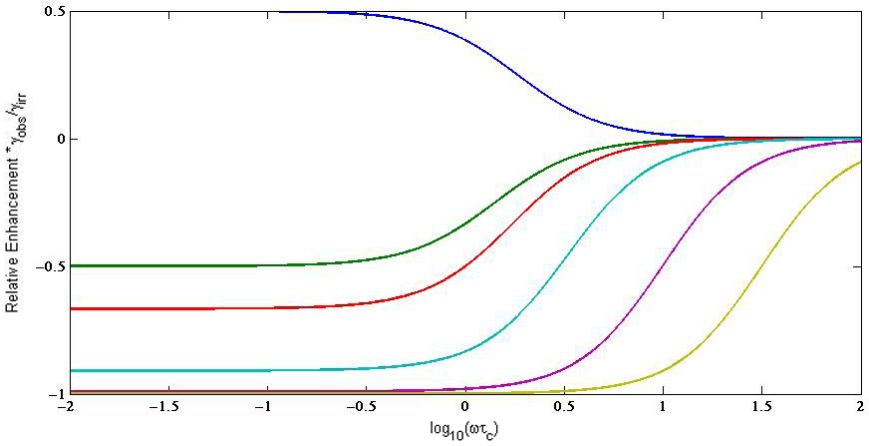

frequency) to the nuclear Larmor frequency. In particular, the electron spins may be spin locked and their nutation frequency under spin lock may be made to match the nuclear Larmor frequency, establishing thereby conditions for polarization transfer: a technique known as **n**uclear spin **o**rientation **v**ia **e**lectron spin **l**ocking (NOVEL)[64–66]. An electron–nuclear cross polarization technique is also known, being termed the **D**ressed **S**tate **S**olid **E**ffect (DSSE)[67].

Temperature dependence

The polarization of a sample of spins is governed by the Curie susceptibility, which is in inverse proportion to the absolute temperature. The precise temperature dependence of the polarization of a spin-1/2 ensemble is briefly discussed below.

It can be shown in reality that with W_0 operative under conditions of ESR saturation, the relative enhancement is a little different for the 1–2 and 3–4 NMR transitions. It turns out that the 3–4 NMR transition, which is a transition between the two highest energy states, is in fact more enhanced, as one might expect. The relative enhancements of the two transitions are given by:

$$\eta_{12} = -\frac{\sinh\left(\frac{\kappa_e}{2}\right)}{\sinh\left(\frac{\kappa_n}{2}\right)} e^{(\kappa_e-\kappa_n)/2} \tag{13}$$

$$\eta_{34} = -\frac{\sinh\left(\frac{\kappa_e}{2}\right)}{\sinh\left(\frac{\kappa_n}{2}\right)} e^{(\kappa_n-\kappa_e)/2} \tag{14}$$

If the two NMR transitions are degenerate, the average of these two enhancements is the one observed.

For the Overhauser effect, therefore, the relative enhancement factor may be shown in fact to be:

$$\eta = \frac{\sinh\left(\frac{\kappa_e}{2}\right)}{\sinh\left(\frac{\kappa_n}{2}\right)} \left[\frac{W_2 \cosh\left(\frac{\kappa_n+\kappa_e}{2}\right) - W_0 \cosh\left(\frac{\kappa_n-\kappa_e}{2}\right)}{(W_2 + 2W_{1n} + W_0 + W^o)} \right] \tag{15}$$

In Eqns. (13) to (15), the parameters κ_e and κ_n are defined as:

$$\kappa_e = \frac{\gamma_e \hbar B_0}{kT}; \quad \kappa_n = \frac{\gamma_n \hbar B_0}{kT} \tag{16}$$

The nuclear polarization scales with temperature as:

$$\frac{\left(1 - e^{-\kappa_n} + e^{\kappa_e} - e^{\kappa_e-\kappa_n}\right)}{\left(1 + e^{-\kappa_n} + e^{\kappa_e} + e^{\kappa_e-\kappa_n}\right)} \tag{17}$$

Since this is approximately in inverse proportion to the absolute temperature T, polarizing at low temperatures and observing at higher temperatures leads to a further enhancement by a factor that is essentially the ratio of the observation temperature to the polarization temperature, provided the warm-up is done adiabatically, conserving spin order.

3. Implementation

Low and moderate field DNP is normally performed in a probe system that includes resonant structures for both the microwaves and radiofrequency waves.

Figure 3: Block diagram of cw X-band DNP spectrometer. The NMR coil (four turns of 28 SWG enameled copper wire wound on a quartz former with id ~5 mm) was located in a cylindrical quartz dielectric cavity. A sealed ampoule of the control sample was employed in the super-regenerative oscillator (SRO) tank circuit [$H_2O/CuSO_4$ for ^1H studies, and $CF_3COOH/Cu(OAc)_2$ for ^{19}F studies]. The SRO is operated in the incoherent mode (where its spectrum is a continuous distribution over a range of frequencies), and makes a transition to the coherent mode when the resonance condition of the control sample is satisfied. One of the two dominant primary responses in the discrete spectrum of the SRO that then results is injected into the RF oscillator for NMR, thereby producing a field-frequency lock. Owing to the use of a broadband RF bridge and a 25.1 MHz IF receiver, 'multinuclear' NMR was possible with this setup, and in our case ^1H and ^{19}F DNP studies could be conveniently carried out. Reproduced from: Rev. Sci. Instr., **52**, 533 (1981)[48]. [Copyright American Institute of Physics.]

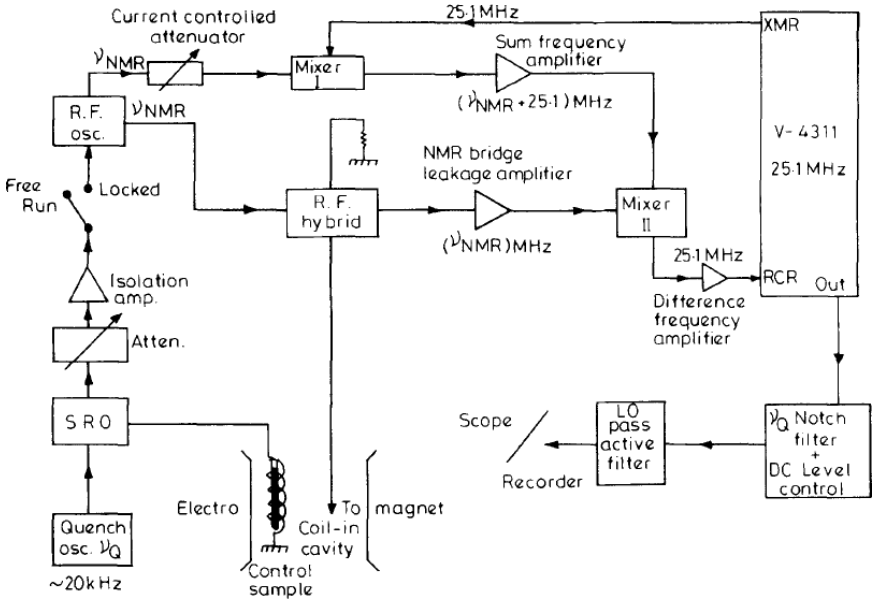

Thus, slow wave structures (e.g., helix), or coil-in-the-cavity arrangements have been frequently employed, the latter preferably involving low *Q* cavities such as dielectric cavities, so that introduction of the coil does not greatly reduce the *Q* factor. Microwave power sources employed for X-band work have generally involved klystrons, IMPATT diodes, or Gunn diode oscillators, their power output being typically of the order of several hundreds of milliwatts.

As an example, we briefly summarize the present author's design and implementation of a cw X-band DNP system[48]. The block diagram of the system is given in Fig. 3, and involves a home-built NMR module mated to a commercial cw EPR spectrometer, field-frequency lock being achieved with another home-built device. It turned out that with the typical EPR electromagnet stability given an ageing power supply, the latter was essential to permit moderate resolution in ^1H NMR at the frequency of 14 MHz – very low by today's standards, but already achieving nevertheless the clear resolution of aliphatic from aromatic protons. Owing to low available microwave power (below 200 mW at the cavity), typical EPR saturation parameters that were reached were *ca*. 0.1, resulting in not more than 10% of the maximum theoretical enhancements.

Fig. 4 shows the mixing scheme employed to ensure IF detection on our spectrometer, rendering it capable of multinuclear operation.

On the other hand, high field DNP brings in its wake the need for high frequency microwave sources that output a fair amount of power. In one class of these experiments, the microwave is directly irradiated on the sample which is housed in the MAS rotor: not involving, however, a resonant structure for the microwaves. Currently gyrotrons appear to be the devices of choice, and are fairly well established for this application in the frequency range from 140 GHz to 460 GHz, delivering *ca*. 10–40 W of microwave power cw. A limitation

Figure 4: Mixing scheme employed in the cw X-band DNP spectrometer. Reproduced from: Rev. Sci. Instr., **52**, 533 (1981)[48]. [Copyright American Institute of Physics.]

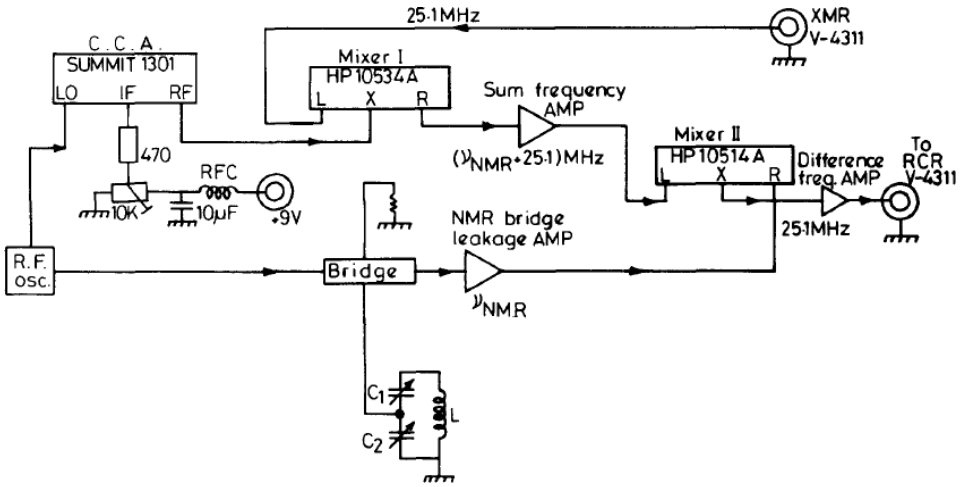

appears to be that the frequency variability of such devices at constant output power is rather severely restricted; one current effort is towards device fabrication offering 1–2 GHz of frequency variability. In practice, it may be noted that a limited microwave frequency tuning range often results in the less than ideal situation of requiring NMR field variation to find the setting for optimum DNP.

One general approach to exploiting high field DNP is to perform low temperature MAS experiments in the solid state, both polarization and detection taking place at the same temperature, in the same phase[42,68].

A fundamentally different approach is to polarize at low temperature in the solid state, then rapidly — adiabatically — melt the polarized sample and investigate it in solution state at ordinary temperatures[69–71]. In the latter context, systems with two vertically 'stacked' co-axial magnets have been designed to enable relatively rapid transfer of the sample from the polarizing field to the NMR field. Alternatively, melting may be performed *in situ* with a laser pulse and the sample recycled for further iterations of DNP, melting and NMR signal acquisition[39]. These approaches may be generically termed 'dissolution DNP', respectively *ex situ* and *in situ*. The application of nuclear spin states such as singlets[71a] that have a long lifetime has been considered for dissolution DNP experiments, exploiting the possibility of storing enhanced nuclear polarization as a long-lived state.

Figure 5: Typical ^{1}H spectral output on our cw X-band DNP system, with and without field-frequency lock, demonstrated on a sample of *m*-xylene/TTBP; microwave off in both cases. Reproduced from: Rev. Sci. Instr., **52**, 533 (1981)[48]. [Copyright American Institute of Physics.]

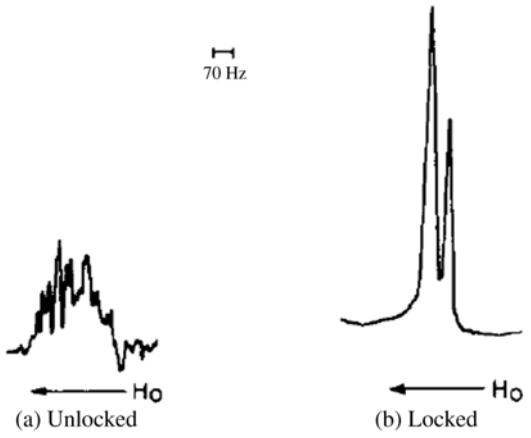

4. Typical results of DNP enhanced high resolution spectroscopy

4.1. *Moderate fields*

We briefly summarize here some of our early results at moderate fields, which threw light on electron density distribution and sigma bond polarizabilities in diamagnetic molecules containing ^{19}F.

The systems investigated comprised the solution of tri-*t*-butylphenoxyl radical (TTBP) at a typical concentration of *ca.* 10^{-2}M in diamagnetic solvents of interest. While the basic stability of the available EPR system did not permit ^{1}H chemical shift resolution even to the extent of *ca.* 5 ppm at *ca.*

Figure 6: ^{1}H DNP in *p*-xylene/TTBP. Spectral traces are shown with the microwave power off (left) and on (right). Note that both aliphatic and aromatic ^{1}H sites show essentially the same negative enhancement, typical of non-selective dipolar interaction. Reproduced from: Rev. Sci. Instr., **52**, 533 (1981)[48]. [Copyright American Institute of Physics.]

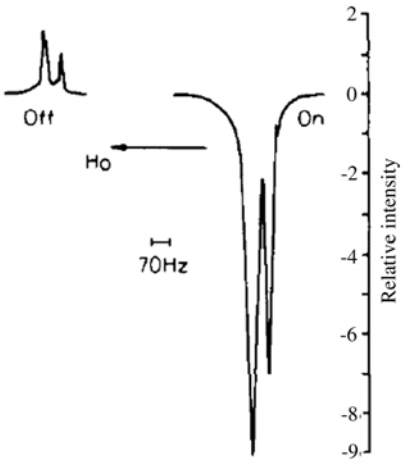

Figure 7: ^{19}F DNP in 1,4-bis(trifluoromethyl)benzene/TTBP. Spectral traces are shown with the microwave power off (left) and on (right). Reproduced from: Rev. Sci. Instr., **52**, 533 (1981)[48]. [Copyright American Institute of Physics.]

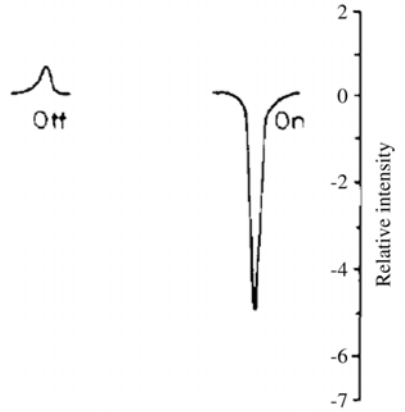

14 MHz, non-spinning resolution of aromatic from aliphatic protons was routinely possible in the presence of the free radical, employing our field-frequency lock module. This is demonstrated in Fig. 5.

Given the microwave power available, with saturation parameters hovering around 0.1, enhancement factors in the range −5 to −20 were achieved on ^{1}H, and in the range −5 to +10 for ^{19}F. A typical example is shown in Figs 6 and 7 for each of the two nuclei, where dipolar interactions dominate the cross-relaxation.

In a number of molecules containing fluorine, particularly interesting results were obtained reflecting differential scalar cross relaxation rates at different ^{19}F sites in the same molecule. Some typical experimental results are shown in Figs 8 and 9.

The general model invoked to interpret the results of such measurements is that ^{1}H DNP is dominated by dipolar interaction modulated by translational diffusion. The 'ultimate–ultimate' enhancement factor U_∞ is deduced from the measurements by extrapolating the linear plot of the reciprocal relative enhancement (η^{-1} or A^{-1}) measured as a function of reciprocal relative microwave power; this then allows the motional correlation time to be inferred. In a molecule that contains both ^{1}H and ^{19}F, the same correlation time would apply for the ^{19}F DNP as well, which then permits the value of U_∞ to be predicted for ^{19}F, based on the model of dipolar interaction. Deviations from this predicted value are then clearly attributable to scalar interactions.

The model that we developed to further interpret the differential enhancements observed for ^{19}F then relies on differential scalar interactions with TTBP. Since TTBP is sterically well-shielded, it is known to interact with the solvent molecules by exchange polarization rather than by specific chemical interactions[72]. Thus, differential scalar interactions are in turn attributable to differential hyperfine couplings, rather than differential scalar correlation times. We found that a model based on the *s* electron density induced at the ^{19}F sites by exchange interaction of the solvent p_σ orbitals with the radical is able to reproduce the qualitative trends of experimental differential enhancements satisfactorily. To this end, we introduced a parameter that we termed the sp_σ polarizability parameter. It was also shown that smaller valence shell electron densities — primarily arising from the p_σ orbital — correlate with higher scalar rates. More explicit models that consider the detailed molecular interaction between the radical solute and the solvent considered as a supermolecule with separations around the relevant van der Waals distance are also possible[46,47,73].

4.2. *High fields*

As noted earlier, CE relies on a three spin electron-electron-nuclear spin flip mechanism that requires: (i) $|\omega_{1e} - \omega_{2e}| = \omega_n$, i.e., that the two EPR frequencies differ by the NMR frequency; as well

Figure 8: ^{19}F DNP in 1,2,4-trifluorobenzene/TTBP. Spectral traces are shown with the microwave off (left) and on (right). Note the clear differential enhancements, the F_4 and F_2 sites showing enhancements of opposite sign. Reproduced from: Mol. Phys., **45**, 179 (1982)[50]. [Copyright Taylor and Francis.]

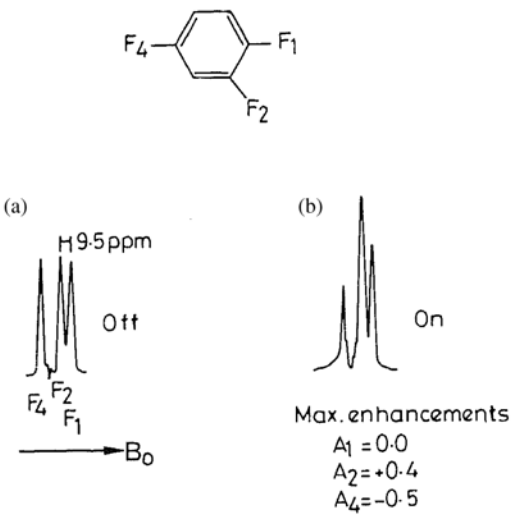

Figure 9: ^{19}F DNP in octafluorotoluene/TTBP. Spectral traces are shown with the microwave off (left) and on (right). Differential enhancements are clearly in evidence, the aliphatic CF_3 fluorines showing strong negative enhancement, while the *m* and *p* fluorines show strong positive enhancements. Reproduced from: Mol. Phys., **45**, 179 (1982)[50]. [Copyright Taylor and Francis.]

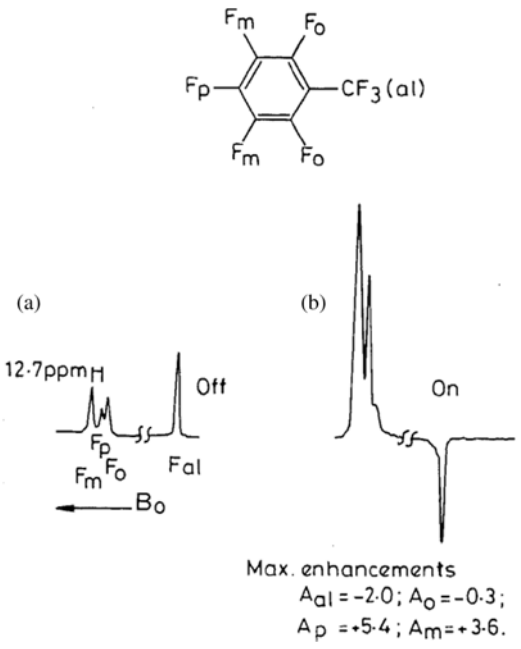

as (ii) a reasonable dipolar interaction between the two electrons. It has proved possible to use a mix of two radicals to satisfy these conditions. As an example, a 50–50 mole % mixture of TEMPO and trityl has been shown to outperform the DNP based on the corresponding individual radicals at the same concentration[40]. Considerable attention is currently being paid however to developing designer biradicals whose two EPR frequencies differ by the NMR frequency and at the same time involve a significant electron-electron dipolar coupling. Tethered biradicals dispersed in a glassy matrix of glycerol/water have turned out to be the current frontrunners. TOTAPOL (1-(TEMPO-4-oxy)-3(TEMPO-4-amino)-propan-2-ol) has proved particularly successful. The 'intramoleuclar' electron-electron dipolar coupling in such systems is about 20 MHz and exceeds by over a factor of 70 the 'intermolecular' electron dipolar coupling between two TEMPO radicals. A promising approach is to try and orient the two electron *g*-tensors appropriately by using a suitable spacer group in the biradical, to satisfy the matching condition. Since the ESR frequency strongly depends on molecular orientation relative to the field — especially at higher fields — the matching condition in a biradical is controlled by the relative orientations of the electron *g*-tensors. A distribution of these relative orientations in turn reduces the efficiency of DNP. In this context, a rigid tether that locks the two nitroxide moieties in a fixed relative orientation would lead to improved performance, compared to a more flexible tether. Thus, it has been recently shown that two TEMPO moieties locked by a bisketal tether, as in the bTbk (bis-TEMPO-bisketal) species, outperforms TOTAPOL[74]. The structures of popular radicals in use for DNP are shown in Fig. 10.

The *g* anisotropy of nitroxide radicals dictates in fact that the two *g*-tensors be orthogonally oriented for optimal DNP performance. Typical concentrations of the biradicals required are *ca*. 10 mM.

It has been shown that MAS studies of arginine and T4 lysozyme at 40–55 K and 5 T, accompanied by electron spin irradiation at *ca*. 140 GHz resulted in DNP enhancements upto a factor of 100. Recent applications of high field DNP relying on the cross effect include the observation of the first NMR spectrum, at 90 K and 9 T, of the K intermediate in the ion-motive photocycle of bacteriorhodopsin. An enhancement factor of 40 was obtained for ^{15}N work, employing the TEMPO free radical[36].

Taking a significant further step in ultrafast NMR, single scan *n*D NMR methods have also been meshed with DNP enhanced spectroscopy. As an

Figure 10: Typical free radicals, including nitroxides and biradicals used for high field DNP.
Top left: TEMPO; Top right: TTBP; Second row from top: left: trityl; right: 4-hydroxy-TEMPO; Third row: bTbk; Bottom: TOTAPOL.

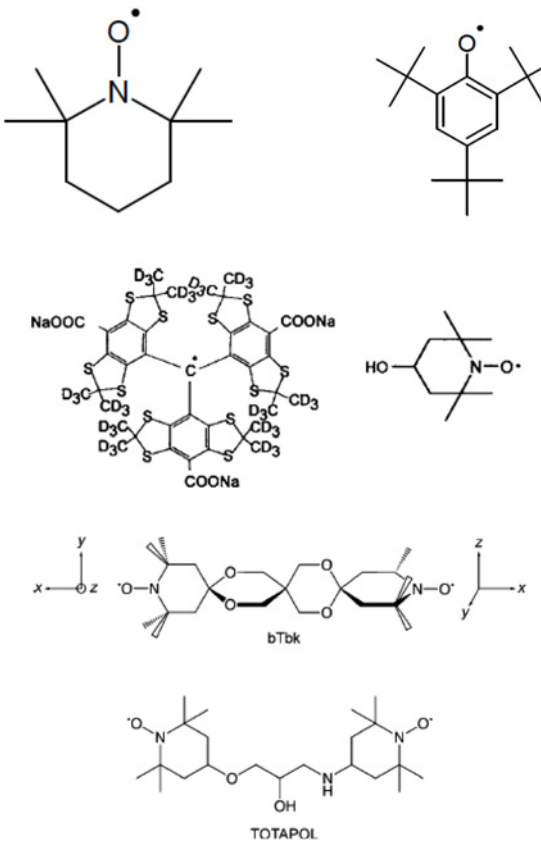

example, DNP enhanced HSQC NMR of pyridine in solution state has been demonstrated, polarizing at 94 GHz and measuring at 7T[75]. 2D spectra of sub-micromolar concentrations in solution could thus be acquired in 0.1 s, the procedure involving *ex situ* DNP and dissolution and transfer of the sample from the polarizing to the measuring field.

5. Outlook

DNP has been extensively employed in the past to study molecular hydrodynamics in solution and also for sensitivity enhanced MR imaging. The extension of DNP from traditional low and moderate fields to high fields clearly throws open a whole vista of untapped potential in a range of applications including the detection of reaction intermediates and the detection of 'impurity' species at low concentration in multi-component systems, in addition of course to the possibility of significant reduction in measurement time. The latter would clearly permit efficient multi-dimensional NMR experiments on complex systems, all the more so when combined with ultrafast *n*D techniques. The dissemination and practice of DNP is however intimately linked to the development of suitable high frequency microwave technology, DNP probe systems, as well as the design of suitable paramagnetic species including free radicals, biradicals and other polarizing agents.

It would appear then that NMR is in the throes of yet another 'rebirth', of the kind which has kept it an evergreen perennial.

Received 15 January 2010; accepted 16 February 2010.

References

1. P. Styles, N. F. Soffe, C. A. Scott, D. A. Cragg, F. Row, D. J. White and P. C. J. White, J. Magn. Reson., **60**, 397 (1984).
2. D. Marek, US Patent 5,247,256: RF Receiver Coil Arrangement for NMR Spectrometers.
3. A. A. Maudsley and R. R. Ernst, Chem. Phys. Lett., **50**, 368 (1977).
4. G. Bodenhausen and R. Freeman, J. Am. Chem. Soc. **100**, 320 (1978).
5. G. A. Morris and R. Freeman, J. Am. Chem. Soc., **101**, 760 (1979).
6. O. W. Sørensen, R. Freeman, T. Frenkiel, T. H. Mareci and R. Schuck, J. Magn. Reson., **46**, 180 (1982).
7. S. W. Sparks and P. D. Ellis, J. Magn. Reson., 62, 1 (1985).
8. I. S. Podkorytov, J. Magn. Reson., **89**, 129 (1990).
9. L. Müller, J. Am. Chem. Soc., **101**, 4481 (1979).
10. A. Bax, R. H. Griffey and B. L. Hawkins, J. Magn. Reson., **55**, 301 (1983).
11. N. Chandrakumar and K. Nagayama, Chem. Phys. Lett., **133**, 288 (1987).
12. P. J. Keller and K. E. Vogele, J. Magn. Reson., **68**, 389 (1986).
13. J. Weigelt and G. Otting, J. Magn. Reson. A, **113**, 128 (1995).
14. B. Reif, M. Köck, R. Kerssebaum, H. Kang, W. Fenical and C. Griesinger, *J*.Magn. Reson. A, **118**, 282 (1996).
15. A. Meissner, D. Moskau, N. C. Nielsen and O. W. Sørensen, J. Magn. Reson., **124**, 245 (1997).
16. K. E. Kövér and P. Forgó, J. Magn. Reson., **166**, 47 (2004).
17. A. W. Overhauser, Phys. Rev., **92**, 411 (1953).
18. T. R. Carver and C. P. Slichter, Phys. Rev., **92**, 212 (1953).
19. T. R. Carver and C. P. Slichter, Phys. Rev., **102**, 975 (1956).
20. R. G. Lawler, Prog. Nucl. Magn. Reson. Spectro., **9**, 147 (1973).
21. P. H. Hore and R.W. Broadhurst, Prog. Nucl. Magn. Reson. Spectro., **25**, 345 (1993).
22. C. R. Bowers and D. P. Weitekamp, Phys. Rev. Lett., **57**, 2645 (1986).
23. J. Natterer and J. Bargon, Prog. Nucl. Magn. Reson. Spectro., **31**, 293 (1997).
24. A. Koch and J. Bargon, Inorg. Chem., **40**, 533 (2001).
25. R. W. Adams, J. A. Aguilar, K. D. Atkinson, M. J. Cowley, P. I. P. Elliott, S. B. Duckett, G. G. R. Green, I. G. Khazal, J. López-Serrano and D. C. Williamson, Science, **323**, 1708 (2009).
26. K. D. Atkinson, M. J. Cowley, S. B. Duckett, P. I. P. Elliott, G. G. R. Green, J. López-Serrano, I. G. Khazal and A. C. Whitwood, Inorg. Chem., **48**, 663 (2009).
27. W. Happer, "Polarization of Noble Gas nuclei with optically pumped alkali metal vapors", Encyclopedia of NMR, 6, 3640 (John Wiley & Sons, 1996).
28. B.M. Goodson, J. Magn. Reson., **155**, 157 (2002).
29. A.-M. Oros and N. J. Shah, Phys. Med. Biol., **49**, R105 (2004).
30. D. Suter, "Optically enhanced Magntic Resonance", Encyclopedia of NMR, **5**, 3376 (John Wiley & Sons, 1996).
31. K. H. Hausser and D. Stehlik, Adv. Magn. Reson., **3**, 79 (1968).

32. R. A. Dwek, R.E. Richards and D. Taylor, Ann. Rev. NMR Spectroscopy, **2**, 293 (1969).
33. W. Müller-Warmuth and K. Meise-Gresch, Adv. Magn. Reson., **11**, 1 (1983).
34. R. D. Bates, Jr., Magn. Reson. Rev., **16**, 237 (1993).
35. D.J. Lurie, "Imaging using the electronic Overhauser Effect", Encyclopedia of NMR, **4**, 2481 (John Wiley & Sons, 1996).
36. M. L. Mak-Jurkauskas, V. S. Bajaj, M. K. Hornstein, M. Belenky, R. G. Griffin and J. Herzfeld, Proc. Natl. Acad. Sci. USA **105**, 883 (2008).
37. N. M. Loening, M. Rosay, V. Weis and R. G. Griffin, J. Am. Chem. Soc. **124,** 8808 (2002).
38. K.-N. Hu, H.-h. Yu, T.M. Swager and R. G. Griffin, J. Am. Chem. Soc. **126**, 10844 (2004).
39. C.-G. Joo, K.-N. Hu, J. A. Bryant and R. G. Griffin, J. Am. Chem. Soc. **128**, 9428 (2006).
40. C. Song, K.-N. Hu, C.-G. Joo, T. M. Swager and R. G. Griffin, J. Am .Chem. Soc. **128**, 11385 (2006).
41. K.-N. Hu, V. S. Bajaj, M. Rosay and R. G. Griffin, J. Chem. Phys., **126**, 044512 (2007)
42. T. Maly, G. T. Debelouchina, V. S. Bajaj, K.-N. Hu, C.-G. Joo, M. L. Mak-Jurkauskas, J. R. Sirigiri, P. C. A. van der Wel, J. Herzfeld, R. J. Temkin and R. G. Griffin, J. Chem. Phys., **128**, 052211 (2008).
43. K.-N. Hu, C. Song, H.-h. Yu, T. M. Swager and R. G. Griffin, J. Chem. Phys. **128**, 052302 (2008).
44. R. K. Gupta, Ph.D. Thesis, I.I.T. Kanpur (196X).
45. S. Aravamudhan, Ph.D. Thesis, I.I.T. Kanpur (1974).
46. N. Chandrakumar, Ph.D. Thesis, I.I.T. Kanpur (1979).
47. A. Tripathi, Ph.D. Thesis, I.I.T. Kanpur (1983).
48. N. Chandrakumar and P. T. Narasimhan, Rev. Sci. Instrum., **52**, 533 (1981).
49. N. Chandrakumar and P. T. Narasimhan, J. Chem. Phys., **77**, 2697 (1982).
50. N. Chandrakumar and P. T. Narasimhan, Mol. Phys., **45**, 179 (1982).
51. P. Hoefer, G. Parigi, C. Luchinat, P. Carl, G. Guthausen, M. Reese, T. Carlomagno, C. Griesinger and M. Bennati, J. Am. Chem. Soc., **130**, 3254 (2008)
52. C.D. Jeffries, Phys. Rev. **106**, 164 (1957).
53. O. S. Leifson and C. D. Jeffries, Phys. Rev., **122**, 1781 (1961).
54. T. J. Schmugge and C. D. Jeffries, Phys. Rev. Lett., **9**, 268 (1962)
55. A. Abragam and W. G. Proctor, Compt. Rend., **246**, 2253 (1958).
56. A. Abragam, J. Combrisson and I. Solomon, Compt. Rend., **247**, 2237 (1958).
57. M. Borghini and A. Abragam, Compt. Rend., **248**, 1803 (1959).
58. A. Henstra, P. Dirksen and W. Th. Wenckebach, Phys. Lett. A, **134**, 134 (1988).
59. C. F. Hwang and D. A. Hill, Phys. Rev. Lett., **18**, 110 (1967).
60. C. F. Hwang and D. A. Hill, Phys. Rev. Lett., **19**, 1011 (1967).
61. D. S. Wollan, Phys. Rev. B, **13**, 3671 (1976).
62. D. S. Wollan, Phys. Rev. B, **13**, 3686 (1976).
63. N. Chandrakumar, Y. Matsuki and T. Fujiwara, private communication.
64. A. Henstra, P. Dirksen, J. Schmidt and W. Th. Wenckebach, J. Magn. Reson. **77**, 389 (1988).
65. A. Henstra and W. Th. Wenckebach, "Nuclear orientation via electron spin locking in Si:B", *in* Pulsed Magnetic Resonance – NMR, ESR and Optics, Ed. D. M. S. Bagguley, Chapter 18, pp. 411 (Clarendon, 1992).
66. H. Brunner, R. H. Fritsch and K. H. Hausser, Z. Naturforsch., **42A**, 1456 (1987).
67. V. Weis and R. G. Griffin, Solid State NMR, **29**, 66 (2006).
68. D. A. Hall, D. C. Maus, G. J. Gerfen, S. J. Inati, L. R. Becerra, F. W. Dahlquist and R. G. Griffin, Science, **276**, 930 (1997).
69. T. Prisner and W. Köckenberger, Appl. Magn. Reson., **34**, 213, (2008).
70. J. H. Ardenkjaer-Larsen, B. Fridlund, A. Gram, G. Hansson, L. Hansson, M. H. Lerche, R. Servin, M. Thaning, and K. Golman, Proc. Natl. Acad. Sci. U.S.A., **100**, 10158 (2003).
71. J. Wolber, F. Ellner, B. Fridlund, A. Gram, H. Johannesson, G. Hansson, L. H. Hansson, M. H. Lerche, S. Mansson, R. Servin, M. Thaning, K. Golman and J. H. Ardenkjaer-Larsen, Nucl. Instrum. Methods Phys. Res., Sect. A, **526**, 173 (2004).

71a. M. Carravetta and M.H. Levitt, J. Am. Chem. Soc., **126**, 6228 (2004).

72. J. A. Potenza and E. H. Poindexter, J. Am. Chem. Soc., **90**, 6309 (1968).
73. A. Tripathi and P. T. Narasimhan, Mol. Phys. **54**, 1415 (1985).
74. Y. Matsuki, T. Maly, O. Ouari, H. Karoui, F. L. Moigne, E. Rizzato, S. Lyubenova, J. Herzfeld, T. Prisner, P. Tordo and R. G. Griffin, Angew. Chem. Int. Ed., **48**, 4996 (2009).
75. L. Frydman, D. Blazina, Nat. Phys., **3**, 415 (2007).

Chandrakumar is Professor of Chemistry at the Indian Institute of Technology-Madras. His research interests include Magnetic Resonance Spectroscopy and Imaging.